MAGNETOHYDRODYNAMICS Vol. 61 (2025), No. 1–2, pp. 199–208
DOI: 10.22364/mhd.61.1–2.21

# NUMERICAL ANALYSIS OF THE EFFECT OF FORCED CONVECTION DRIVEN BY TRAVELING MAGNETIC FIELD ON THE CRYSTAL GROWTH OF SILICON BY CZOCHRALSKI TECHNIQUE

*D. Kehili*[1*], *B. Hiba*[1*], *Ab. Nouri*[1], *K. Zaidat*[2], *L. Hachani*[1]

[1] *Laboratoire Physique des Matériaux, Université Amar Telidji de Laghouat, BP 37G, Laghouat, 03000, Algérie*
[2] *SIMaP -UJF 5266 Domaine Universitaire, BP 75- 38402 Saint Martin d'Hères, France*
**e-Mails: b.hiba@lagh-univ.dz, d.kehili.mec@lagh-univ.dz*

A numerical simulation of silicon crystal growth in a specific Czochralski furnace was carried out. The experimental process involves a melting stage, a holding stage to homogenize the melt by electromagnetic stirring and, finally, a solidification stage by pulling the seed upwards to obtain a single crystal. Enthalpy formulation with moved and deformed mesh technique is used for numerical simulations of the phase-change problems. However, only the stage of solidification under the effect for forced convection driven by an external travelling magnetic field was numerically investigated. The proposed numerical model has demonstrated its effectiveness in predicting the effect of electromagnetic stirring on the solidification process in terms of thermal field, dynamic field and shape and localization of the solidification front. Unfortunately, due to the lack of experimental measurements, the results obtained by numerical simulation have not been yet validated.

**Introduction.**

Numerical simulation plays an important role in the growth of silicon crystals by the Czochralski (CZ) technique, a crucial process in the semiconductor industry [1–4]. The CZ method, used widely to grow single crystal silicon of high-purity for electronic devices, demands accurate control across multiple parameters to guarantee the quality and uniformity of the single crystals. By employing numerical simulation, scientists can forecast scenarios of the physical system under different conditions by setting the parameters of the process and detect possible problems before they emerge in the real production environment [5–7]. Numerical simulation enables for a comprehensive analysis of heat transfer and fluid mechanics in the melt and crystal, which are significant for understanding the phase change problem, hydrodynamic movements, and the shape of the solidification front. This forecasting ability assists in effectively setting the temperature, rotation rates, and pulling velocities, resulting in improved crystal quality and in minimizing flaws. Moreover, simulation helps in the design and enhancing of crystal growth equipment, guaranteeing that new setups satisfy the rigorous requirements of the industry without the necessity of extensive experiments [8–10]. In addition, the employment of numerical simulation contributes to resource conservation and cost reduction. By simulating different scenarios, companies can reduce energy consumption, minimize material waste, and expedite the production of single crystals. Also numerical simulation improves the economic viability of crystal production and sustains the development of semiconductor technologies by allowing the manufacture of superior-quality silicon crystals [1, 11, 12]. In this paper, we present a 2D numerical simulation of the effect of magnetohydrodynamic (MHD) flow in a cylindrical crucible driven by a travelling magnetic field (TMF) on the crystal growth of single crystalline silicon ingot using the Czochralski technique.

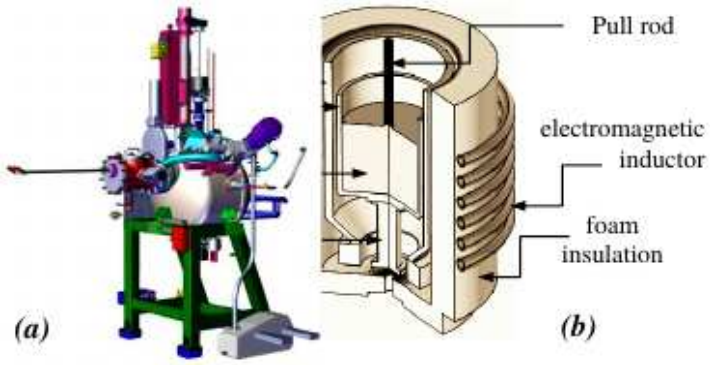


*Fig. 1.* (*a*) The Czochralski furnace used in experiment with the mean components; (*b*) schematic of the studied system.

**1. Problem formulation.**

In this work, the interaction of electromagnetism, fluid mechanics and heat transfer including phase change (solidification in our case) during the CZ growth process was modelled. Furthermore, pulling by a pull rod was approximated, and the free surface shape was considered in the geometry modelling. For this purpose, the developed numerical model is focused on a particular CZ furnace manufactured by Krystalix in SIMaP laboratory of Grenoble (France).

As shown in Fig. 1, the numerically studied system is mainly composed of silicon contained in a cylindrical fused silica crucible of 10 cm in diameter, which is partially filled (6 cm high) and held by a graphite support surrounded by an electromagnetic inductor (the source of TMF), a multi-layer foam insulation treated several times by high temperature annealing (1600°C) before the pulling stage, and a special coating to avoid any possibility of contamination gases. In addition, a seed crystal is mounted on a movable pull rod quenched on the surface of molten silicon at a temperature just above the melting point 1414°C. The inductor is supplied with three-phase currents shifted by $2\pi/3$ at a network frequency $f_0 = 50$ Hz to generate a travelling magnetic field which in turn creates a controlled MHD flow in the liquid phase during the solidification process. When all silicon is molten and a homogeneous temperature is reached by electromagnetic stirring, the rotating seed crystal is moved downwards and dipped into the melt, where it locally cools the liquid silicon. It solidifies with the same crystal structure as the seed, which is then slowly pulled upwards with a rate of 5 mm/h and simultaneously rotated at 5 rev/min to maintain a constant position of the interface between the crystal and the melt. At the end of the process, the crystal is detached from the residual melt and cooled down to ambient temperature in a controlled way.

**2. Numerical model.**

The developed numerical model is focused on simulating the growth process, for which electromagnetism in a harmonic regime, unsteady-state heat transfer and phase change, and transient melt flow are considered. Additionally, a 2D axisymmetric model geometry of the CZ furnace was adopted using the Comsol Multiphysics$^{TM}$software simulation. Indeed, despite the relatively high Reynolds number of the melt prior to solidification clearly indicating the turbulent regime, as soon as the pulling process evolves, the velocities decrease significantly leading to lower Reynolds numbers and consequently to the transition to a weakly turbulent regime over time. Furthermore, the large-scale flow

patterns remain predominantly axisymmetric, supporting the use of a 2D axisymmetric approach to effectively capture the primary flow dynamics. The phase change problem was solved using the enthalpy approach based on an apparent heat capacity method, which computed the position of the crystallization front using the liquid fraction predicted by the melting point and the latent heat release. The crystal-melt boundary was moved into this new position using the deformed mesh solver, which applied elastic deformation based on a given displacement of the boundaries to update the geometry.

*2.1. Physical equations.* When modeling the CZ crystal growth, different physical phenomena described by mathematical equations need to be considered. These equations are presented in the following sections and the modelling assumptions required in their derivation are discussed.

*2.1.1. Electromagnetic part.* As it is well known, the use of the vector potential or *A-V* formulation with the vector potential $\mathbf{A}$ and the scalar potential $V$ is advantageous for the description of electromagnetic problems because it reduces the number of Maxwell unknowns and equations to four and two, respectively. These potentials are defined as

$$\begin{cases} \mathbf{B} = \boldsymbol{\nabla} \times \mathbf{A}, \\ \mathbf{E} = \partial \mathbf{A}/\partial t + \nabla V. \end{cases} \tag{1}$$

The equation system for calculating these potentials, using the simplified equations ($\boldsymbol{\nabla} \cdot \mathbf{B}$=0) and ($\mathbf{J}$=$\sigma\mathbf{E}$), is then given by

$$\begin{cases} \boldsymbol{\nabla} \times \dfrac{1}{\mu_\mathrm{e}} \boldsymbol{\nabla} \times \mathbf{A} = \mathbf{J} = \sigma_\mathrm{elec} \left(\partial \mathbf{A}/\partial t + \nabla V\right) + \mathbf{J}_\mathrm{s}, \\ \boldsymbol{\nabla} \cdot \left(\sigma_\mathrm{elec} \left(\partial \mathbf{A}/\partial t + \nabla V\right)\right) = 0. \end{cases} \tag{2}$$

where $\mathbf{A}$ is the magnetic vector potential, $\sigma_\mathrm{elec}$ is the electrical conductivity, $\mu_\mathrm{e} = \mu_0 \mu_\mathrm{r}$ is the magnetic permeability, $\mu_0$ is the permeability of free space ($4\pi \times 10^{-7}\,\mathrm{N/A^2}$), and $\mu_\mathrm{r}$ is the relative permeability. The $V$ is the electric scalar potential, $\mathbf{J}$=$\sigma_\mathrm{elec}\left(\mathbf{E} + \mathbf{u} \times \mathbf{B}\right)$ is the current density vector given by Ohm's law, $\mathbf{J}_\mathrm{s}$ is the applied source of the current density vector; $\mathbf{E}$ is the electric field intensity vector, $\mathbf{u}$ is the velocity of the melt and, finally, $\mathbf{B}$ is the induced magnetic field. Furthermore, electromagnetic modelling is required to compute the Lorentz forces influencing the melt flow in a multiphysical manner.

*2.1.2. Heat transfer.* Heat transfer modelling is a fundamental part of the CZ growth simulation, as the temperature distribution in the furnace is crucial for the phase change between the crystal and the melt, i.e. it is a relevant parameter of the process. Different mechanisms of heat transfer have to be considered: heat conduction, heat convection, and thermal radiation. Furthermore, for pure silicon, the interface between the liquid and the solid phase of the same material exists, it is the so-called solidification front or crystallization interface. Under the assumption of negligible superheating or undercooling, this interface is simulated as a diffuse interface. Moreover, due to the change in atomic arrangement during solidification, latent heat is released leading to a sudden jump in heat flux at the solidification front. This is described by the following equation:

$$\frac{\partial(\rho C_p T)}{\partial t} + \frac{\partial(\rho f_\mathrm{l} L)}{\partial t} = -\nabla(\rho u h) + \nabla(\lambda \nabla T), \tag{3}$$

where $\rho$ is the density, $\lambda$ is the thermal conductivity, $C_p$ is the apparent heat capacity given by Eq. (5), $L$ is the latent heat, and $f_\mathrm{l}$ is the liquid fraction defined as follows:

$$f_\mathrm{l} = \begin{cases} 0 & \text{for } T < T_\mathrm{m} - \dfrac{1}{2}\Delta T \text{ (solid phase)}, \\ \dfrac{T - (T_\mathrm{m} - \Delta T/2)}{\Delta T} & \text{for } T_\mathrm{m} + \dfrac{1}{2}\Delta T \geq T \geq T_\mathrm{m} - \dfrac{1}{2}\Delta T \text{ (diffuse interface)}, \\ 1 & \text{for } T > T_\mathrm{m} + \dfrac{1}{2}\Delta T \text{ (liquid phase)}, \end{cases} \tag{4}$$

with $T_\mathrm{m}$ being the melting temperature of silicon and $\Delta T$ the half-width of temperature transition, and

$$C_p(T) = C_{p\mathrm{s}} + f_\mathrm{l}(T)(C_{p\mathrm{l}} - C_{p\mathrm{s}}) + \frac{1}{\sqrt{\pi}\Delta T/4} \exp\left\{ - \left( \frac{T - T_\mathrm{m}}{\Delta T/4} \right)^2 \right\} L, \tag{5}$$

where $C_{p\mathrm{s}}$ is the heat capacity of solid silicon, $C_{p\mathrm{l}}$ is the specific heat of liquid silicon, and $L$ stands for latent heat.

*2.1.3. Heat transfer in solid parts.* The resistor produces heat energy by converting electric power to thermal energy by the Joule effect which is transferred mainly by radiation to the other solid parts of the furnace, namely, the crucible containing the silicon. The corresponding energy equation reads

$$\frac{\partial(\rho C_p T)}{\partial t} = \nabla(\lambda \nabla T) + Q, \tag{6}$$

with

$$Q = \begin{cases} \dfrac{J^2}{\sigma_\mathrm{elec}} & \text{only in the graphite resistor}, \\ 0 & \text{other solid parts}, \end{cases} \tag{7}$$

and

$$Q_\mathrm{rad} = FA\sigma\varepsilon \left( T_1^4 - T_2^4 \right), \tag{8}$$

with $F$ being the radiation configuration factor, $A$ the surface area of the object, $\sigma$=5.67 $\times$ 10$^{-8}$ J/(s·m$^2$K$^2$) is the Stefan–Boltzmann constant, and $\varepsilon$ is the emissivity of the object. The $Q_\mathrm{rad}$ is implemented as the thermal boundary condition in the modified heat transfer formulation dealing with the phase change of silicon.

*2.1.4. Fluid mechanics part.* The resulting MHD configuration is an important factor in the CZ growth as it significantly influences the heat transfer in the melt and hence the position and the morphology of the liquid-solid interface, i.e. it significantly affects the control of the crystal growth process. Since the numerical model is based on the enthalpy approach dealing with all existing phases simultaneously in the computational domain, the Navier–Stokes equation requires necessary modifications to take into account the presence of the solid phase. Indeed, all terms are multiplied by the liquid fraction, on the one hand, and a Carman-Kozeny term is added to dampen the velocity during the transition from liquid to solid state, on the other hand. Furthermore, silicon in the liquid state is considered as an electrically conducting fluid, and when it is exposed to a magnetic field, Lorentz forces arise acting as supplementary body forces which are responsible for the electromagnetic stirring of the melt. A full-scale inductor (Fig. 1*b*) was built to perform an electromagnetic calculation using AC/DC electromagnetic fields

in the commercial COMSOL Multiphysics software. Firstly, the travelling magnetic field $B$ in a harmonic regime was calculated using the frequency-domain solver. The time-averaged $F_{\mathrm{LTZ}}$ was calculated by solving Maxwell's equations, and the extracted $F_{\mathrm{LTZ}}$ was interpolated into the COMSOL turbulent flow solver. Lorentz forces were determined by the liquid fraction $f_{\mathrm{l}}$ and used as a source term in the momentum conservation equations for the liquid phase, Eqs. (9) and (10). Unlike the electromagnetic field calculation, only the casting domain was solved for the flow and solidification.

$$\rho_{\mathrm{l}}\left[\frac{\partial \mathbf{u}}{\partial t}+\frac{1}{f_{\mathrm{l}}}(\mathbf{u}\nabla)\mathbf{u}\right]-\nabla(\mu_{\mathrm{l}}\nabla\mathbf{u})+A_{\mathrm{mash}}\frac{(1-f_{\mathrm{l}})^2}{f_{\mathrm{l}}^3+\varepsilon_0}\mathbf{u}=-f_{\mathrm{l}}\,\mathrm{grad}(p)+f_{\mathrm{l}}\langle F_{\mathrm{LTZ}}\rangle, \tag{9}$$

where $A_{\mathrm{m}}=10^6\,\mathrm{kg/(m^3s)}$ is the mushy zone constant, $f_{\mathrm{l}}$ is the liquid fraction defined by Eq. (4), and $\varepsilon_0=10^{-3}$ is a small positive calculation constant defined to avoid division by zero in the solid state ($f_{\mathrm{l}}=0$) [13]. The time average Lorenz force density is expressed as

$$F_{\mathrm{LTZ}}=\frac{1}{2}\left(\mathbf{J}\times\mathbf{B}\right). \tag{10}$$

*2.2. Free surface and meniscus zone.* In the context of CZ growth, the rise of the liquid melt at the crystal, i.e. the meniscus, is an important factor influencing the local temperature distribution both in the melt and in the crystal. Thus, it requires special attention in physical modelling. Due to the hydrostatic pressure and surface tension, the free surface of the melted silicon is deformed and consequently its height and radius change during the process along the $z$- and $r$-direction, respectively. The relation between the surface tension and the meniscus zone given by the Young–Laplace equation reads

$$\rho g h=\delta\left(\frac{1}{R_2}+\frac{1}{R_1}\right), \tag{11}$$

where $\rho$ is the density, $g$ is the gravity, $h$ denotes the meniscus height, $\delta$ is the surface tension, $R_1$ and $R_2$ are the principal radii of the meniscus curvature.

*2.3. Triple point.* The position of the triple point (TP) is calculated as the intersection of the crystallization interface tangent and the line which forms an angle with the vertical direction at TP (see Fig. 2), where $\beta$ is the so-called growth angle. In fact, this triple point is used as an adjustment parameter in modelling so that the thermal sources are supposed to satisfy the condition that the temperature of this triple point is equal to the melting temperature.

## 3. Moving mesh and crystallization interface.

Numerous mesh refinements were used to examine the accuracy of the model implemented, and minimal refinement was used to ensure the convergence of the solution.

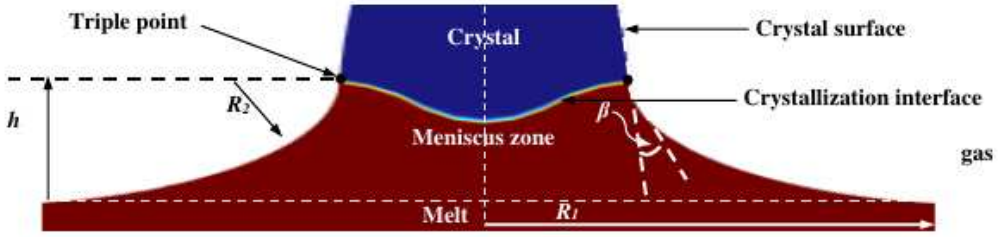


*Fig. 2.* Schematic visualization of the variables for calculating the meniscus shape of the CZ process.

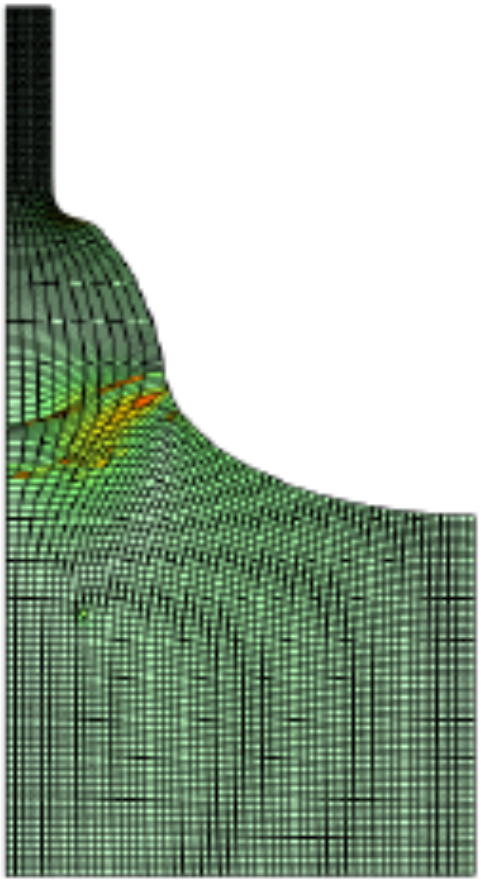

*Fig. 3.* Moving mesh technique in 2D axisymmetric geometry during the CZ process.

*Table 1.* Mesh characteristics.

| Triangles | Quads | Edge elements | Vertex elements | Number of elements | Mesh area |
|---|---|---|---|---|---|
| 798 | 11275 | 958 | 15 | 12073 | 23400 mm$^2$ |

Thus, in this study, except the crucible, we have chosen a quadratic mesh with a particular refinement in the pull rod, as illustrated in Fig. 3. The mesh characteristics are summarized in Table 1. Furthermore, to implement the change in the overall melt shape, a moving mesh was used to calculate the time-dependent crystallization interface as well as the crystal shape and growth for each time step $\Delta t$. This approach allows both the deformation of the mesh and the tracking of the solid-liquid interface once the condition at the interface is well set. The crystallization interface is moved in normal direction (the normal vector $\mathbf{n}$ is shown in Fig. 3) by the distance $v_{\mathrm{n}}\nabla t$. The front normal velocity $v_{\mathrm{n}}$ is calculated from the local heat balance condition after solving the temperature radiation problem and obtaining the heat flux densities at the crystallization interface in the crystal and in the melt ($q_{\mathrm{c}}$ and $q_{\mathrm{m}}$, $q = \lambda \partial T/\partial n$),

$$v_{\mathrm{n}} = \frac{q_{\mathrm{c}} - q_{\mathrm{m}}}{\rho_{\mathrm{c}} L} - \mathbf{V}_{\mathrm{p}}\mathbf{n}, \tag{12}$$

where $L$ is the latent heat of fusion, $\rho_c$ is the crystal density, and $\mathbf{V}_p$ is the crystal pulling rate [14].

The Fig. 3 illustrates also the deformation of the mesh during the Czochralski process. It clearly shows the change in the geometry and size of the elements, where it shrinks in the melt region and stretches in the crystal region to ensure the conservation of mass and volume of silicon when the volume decreases in the melt and increases in the crystal, taking into account the curvature of the free surface.

**4. Results.**

*4.1. Electromagnetic field.* This section discusses the numerical results of the electromagnetic calculation obtained by solving the set of Maxwell's equations in a harmonic mode for the electromagnetic inductor based on the A-V potential formulation and considering the Coulomb gauge condition ($\nabla \mathbf{A} = 0$) to calculate the generated TMF and subsequently the Lorentz force induced in the liquid silicon volume. The results presented in the next sections were obtained for the input surface current density $J = 6000$ A/m and network frequency 50 Hz for electromagnetic stirring purpose only.

The electromagnetic results obtained with the proposed model using the COMSOL software are presented in Fig. 4. These results show the ability of this model to predict the generated TMF configuration (Fig. 4*b*). The results obtained indicate that the maximum magnitude of the induced magnetic field can reach 100 mT near the electromagnetic inductor coil. The Lorentz forces were directed downwards and pointed into

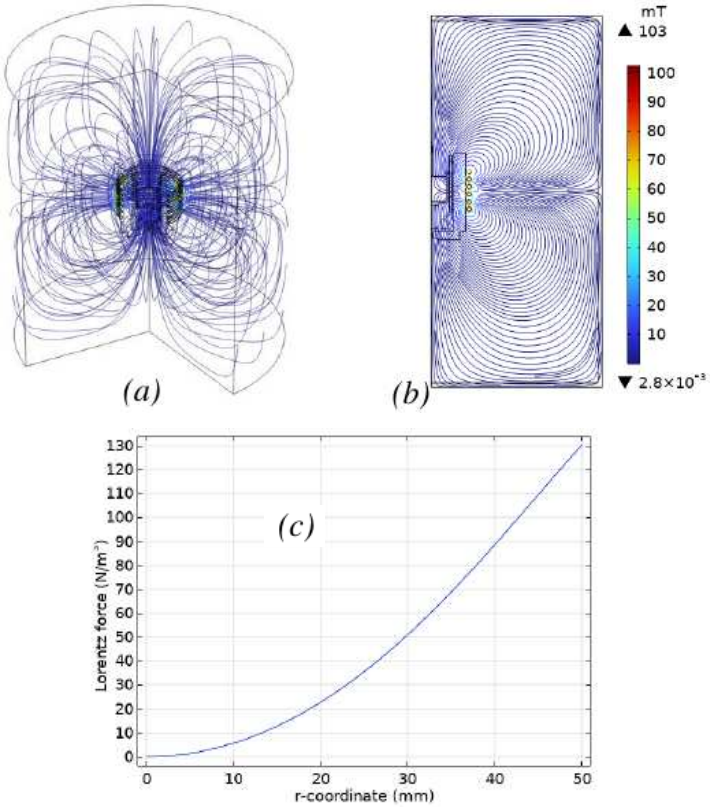


*Fig. 4.* (*a*) 2D revolution at phase ($\phi = 0°$) and (*b*) 2D evolution of the induced magnetic field magnitude, (*c*) evolution of the Lorentz force density averaged in time in the radial direction.

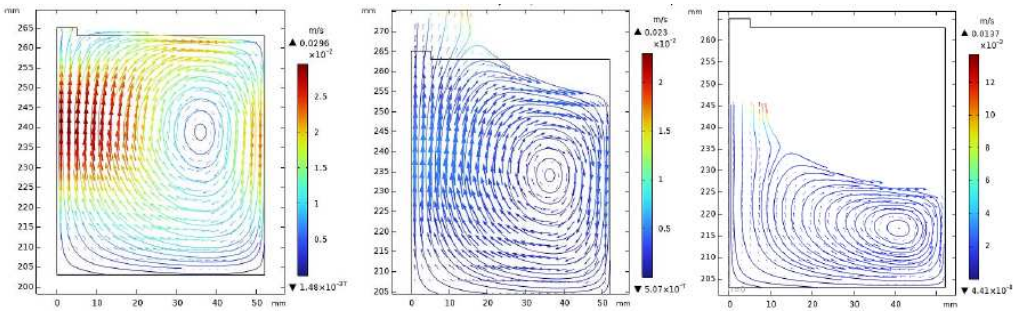

(*a*) (*b*) (*c*)

*Fig. 5.* Velocity vectors at selected times: (*a*) $t = 0\,\mathrm{h}$, (*b*) $t = 10\,\mathrm{h}$ and (*c*) $t = 24\,\mathrm{h}$ during silicon crystal growth.

the melt volume with a maximum magnitude of $130\,\mathrm{N/m^3}$. As illustrated in Fig. 4*c*, the $z$-component of the Lorentz force decreases exponentially with respect to the depth ($r$-direction).

*4.2. Velocity field.* The velocity fields generated by electromagnetic stirring in the melt during the Czochralski process is shown in Fig. 5. The streamlines coupled to the velocity vectors show clearly the effect of the TMF-generated Lorenz forces on the resulting dynamic field in the molten silicon during the Czochralski process at different selected instants 0 h, 10 h and 24 h. The resulting MHD configuration consists of a torus flow exhibited by two dominant vortices distributed symmetrically throughout the crucible, as illustrated in Fig. 5*a*. The maximum value obtained numerically $U_{\max} = 3\,\mathrm{cm/s}$ gives, as expected, a quite high value of the Reynolds number

$$\mathrm{Re} = \frac{\rho U_{\max}\left(H^2/D\right)}{\mu} \cong 3736, \tag{13}$$

where $H$ is the height and $D$ is the diameter of the crucible, which indicates clearly that the flow is turbulent in the beginning before the pulling, i.e. the cooling process.

The velocity starts to decreases when the solidification process begins at about 23 mm/s (Fig. 5*b*) due to the change in the viscous forces, which are influenced by the temperature decrease, and reaches a minimum value at about 13.7 mm/s (Fig. 5*c*) when the temperature in the bath becomes close to the melting temperature and also when the melt volume in the bath reduces and a single crystal starts growing.

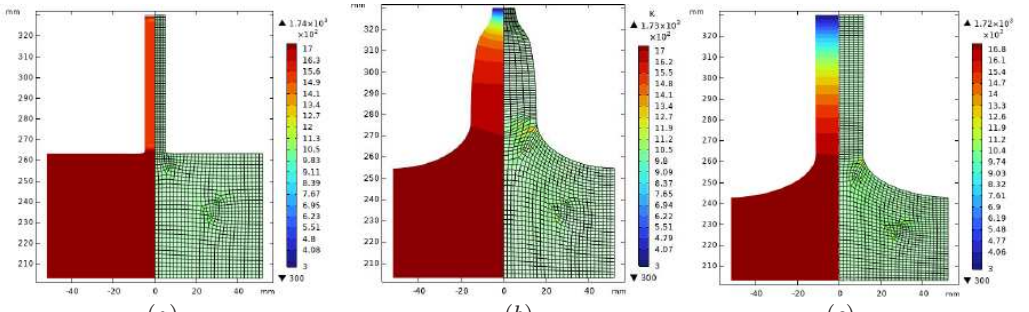

(*a*) (*b*) (*c*)

*Fig. 6.* Velocity vectors at selected times: Finite element mesh and temperature distribution within the melt and crystal at selected times: (*a*) $t = 0\,\mathrm{h}$, (*b*) $t = 10\,\mathrm{h}$ and (*c*) $t = 24\,\mathrm{h}$.

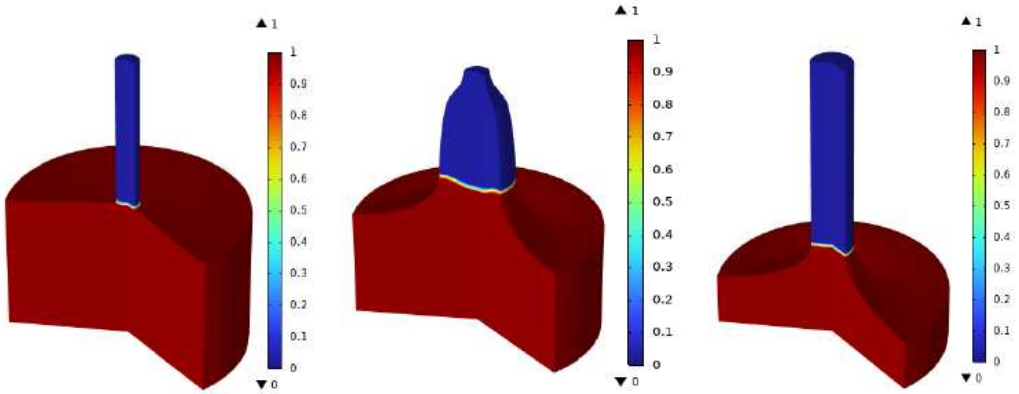


(*a*) (*b*) (*c*)

*Fig. 7.* Liquid fraction positions at selected times: (*a*) $t = 0$ h, (*b*) $t = 10$ h, and (*c*) $t = 24$ h during crystal growth.

*4.3. Temperature field.* The Fig. 6 shows the temperature maps coupled to their corresponding unstructured finite element mesh, involving the crystal and the melt for three subsequent time instants of the calculation: $t = 0$ h (initial geometry); $t = 10$ h (intermediate state corresponding to the cone growth) and, finally, $t = 24$ h corresponds to the transition from cone to cylinder (i.e. shouldering). The melt at a temperature of around $T_{\text{melt}} = 1737$ K is homogenized by electromagnetic stirring before the pulling process begins. The moving mesh interface generates relatively larger quadratic cells in the areas away from the crystallization interface to minimize the computation time. The temperature decreases in the single crystal in the radial direction, where the highest temperature around 1620 K is located in the region closest to the melt (Fig. 6*b*) and the lowest one around 406 K is located in the region farthest from the melt (Fig. 6*c*) creating graduation of the temperature along the single crystal.

*4.4. Liquid fraction.* Fig. 7 shows the localization and shape of the solidification front during the Czochralski process. The 3D evolution of the solidification front exhibits a convex shape (bulging towards the melt) of the silicon during the Czochralski process, then it moves according to the Stephan velocity formula in the upward direction parallel to the direction of the pulling rate and perpendicular to the melt level when the process starts, then it moves downwards. However, when the single crystal forms, the level of the melt decreases with a varying rate by the same amount of the volume ratio in the single crystal formed. In fact, Fig. 6*b*, corresponding to 10 h of pulling, shows that the total melt decreases by about 18%, however, after 24 h (Fig. 6*c*) the melt level indicates a reduction of around 63%. These results were obtained for the pulling rate of around 5 mm/h and rotational velocity of the seed of 5 rev/min.

**Conclusion.**

In this work, the Czochralski crystal growth process has been modelled and investigated. A 2D axisymmetric model was implemented in the COMSOL Multiphysics software to simulate the single crystal growth of silicon by the Czochralski technique under forced convection generated by electromagnetic stirring. The upward and rotational movements of the crystal accompanied by the decreasing melt level were studied using strong coupling between different physics, namely, fluid mechanics involving a modified Navier-Stokes equation, electromagnetism based on the A-V potential formulation, and heat transfer, including the phase change by the enthalpy approach and using a moving mesh tech-

nique. The proposed numerical model has demonstrated its effectiveness in predicting the effect of electromagnetic stirring on the solidification process in terms of the thermal field, dynamic field, shape and localization of the solidification front.

**References**

[1] C. Lan. Twenty years crystal growth of solar silicon: My serendipity journey. *J. Crystal Growth*, (2024).

[2] B. Gao *et al.* Global simulation of coupled carbon and oxygen transport in a Czochralski furnace for silicon crystal growth. *J. Crystal Growth*, (2010).

[3] M. Chatelain. Numerical method for thermal donor formation simulation during silicon Czochralski growth. *Sol. Energy Mater. Sol. Cells*, (2021).

[4] F. Dupret. Global modelling of heat transfer in crystal growth furnaces. *Int. J. Heat Mass Transf.*, (1990).

[5] A. Virzi. Computer modelling of heat transfer in Czochralski silicon crystal growth. *J. Crystal Growth*, (1991).

[6] S. Togawa. Oxygen transport from a silica crucible in Czochralski silicon growth. *J. Crystal Growth*, (1996).

[7] R. Assaker *et al.* Time-dependent simulation of the growth of large silicon crystals by the Czochralski technique using a turbulent model for melt convection. *J. Crystal Growth*, (1997).

[8] A. Smirnov *et al.* Development of oxygen transport model in Czochralski growth of silicon crystals. *J. Crystal Growth*, (2008).

[9] Y.-J. Huang *et al.* A cost-effective approach for transitioning to larger wafer production by small Czochralski pullers. *J. Crystal Growth*, (2024).

[10] W. Zulehner. Historical overview of silicon crystal pulling development. *Mater. Sci. Eng. B*, (2000).

[11] T. Sinno. Defect engineering of Czochralski single-crystal silicon. *Mater. Sci. Eng. R. Rep.*, (2000).

[12] J. Derby *et al.* Thermal-capillary analysis of Czochralski and liquid encapsulated Czochralski crystal growth: I. Simulation. *J. Crystal Growth*, (1986).

[13] B. Hiba, Ab. Nouri, L. Hachani, K. Zaidat. Numerical study of the Bridgman directional solidification process of photovoltaic silicon ingot using power control technique *Magnetohydrodynamics*, vol. 59 (2023), no. 3/4, pp. 401–414; DOI: 10.22364/mhd.59.3-4.12 .

[14] A. Sabanskis, K. Bergfelds, A. Muiznieks, Th. Schröck, A. Krauze. *J. Crystal Growth*, (2013).

Received 24.11.2024